Volume 61
Number 23
21 March 2025
Pages 4419–4576

ChemComm

Chemical Communications

rsc.li/chemcomm

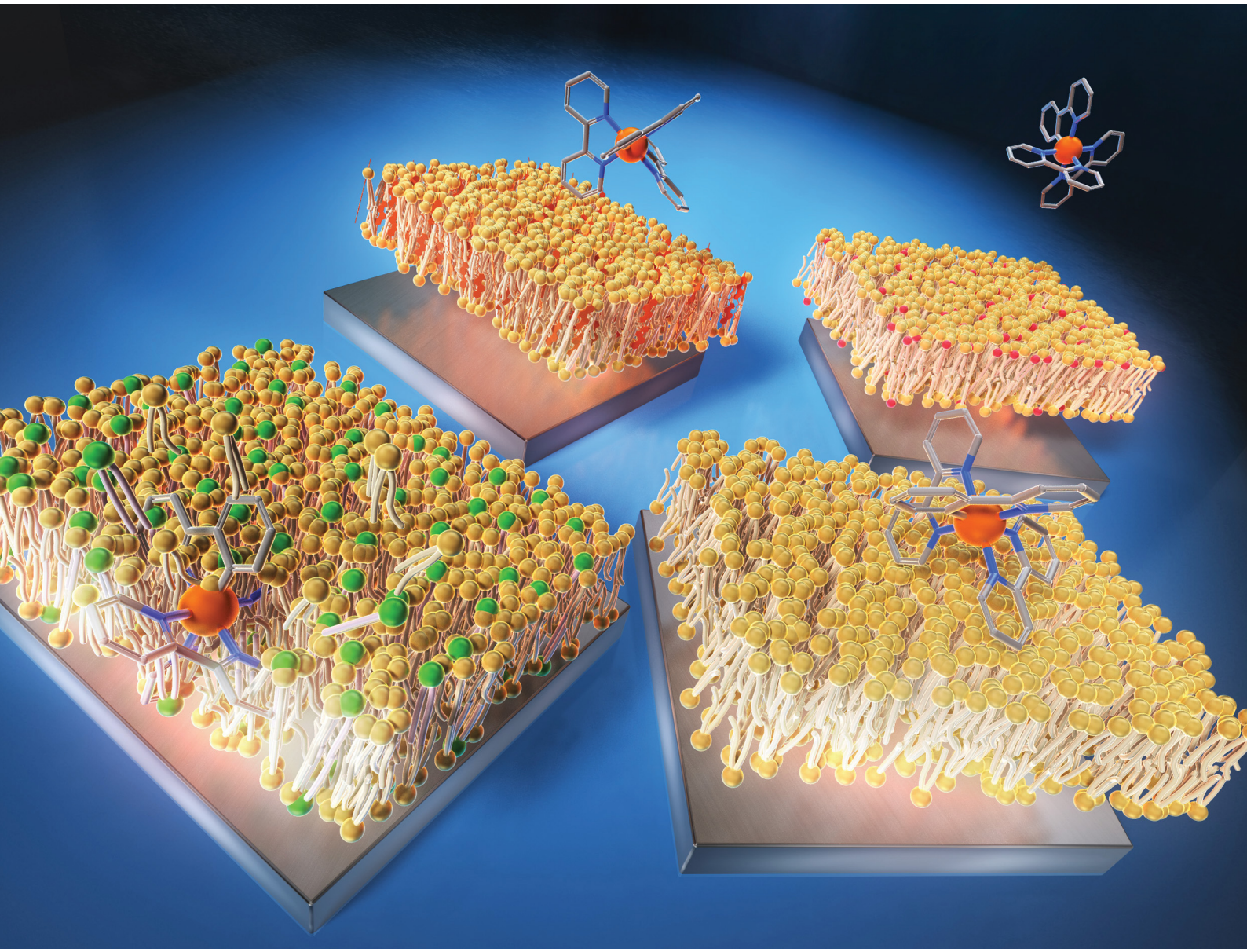

ISSN 1359-7345

ROYAL SOCIETY OF CHEMISTRY

COMMUNICATION

Kaoru Hiramoto *et al.*

Electrochemiluminescence of $[Ru(bpy)_3]^{2+}$/tri-*n*-propylamine to visualize different lipid compositions in supported lipid membranes

ChemComm

COMMUNICATION

View Article Online
View Journal | View Issue

Cite this: *Chem. Commun.*, 2025, **61**, 4495

Received 24th November 2024,
Accepted 31st January 2025

DOI: 10.1039/d4cc06245k

rsc.li/chemcomm

Electrochemiluminescence of $[Ru(bpy)_3]^{2+}$/tri-*n*-propylamine to visualize different lipid compositions in supported lipid membranes†

Kaoru Hiramoto, *[ab] Ayumi Hirano-Iwata, [bc] Kosuke Ino [d] and Hitoshi Shiku [d]

We report the direct imaging of supported lipid membranes using electrochemiluminescence (ECL) of $[Ru(bpy)_3]^{2+}$ and tri-*n*-propylamine (TPrA). Lipid membranes with different compositions exhibited inherent ECL emissions due to electrostatic interactions and altered permeability of the luminophores, demonstrating the promising use of ECL microscopy for lipid membrane studies.

Electrochemiluminescence (ECL) is a light-emitting process through electron transfer between electrodes and luminescent molecules in a solution.[1] Recently, the microscopic use of ECL for (bio)imaging has emerged,[2,3] as ECL has several advantages such as low background signal, high surface sensitivity, and temporal/spatial controllability with voltage application. Given that ECL occurs at the very vicinity of the electrode surface, it is suitable for imaging single entities and/or thin materials on an electrode.[4] Significant reports include observations of single cells,[5] organelles,[6] nanoparticles,[4] and liposomes,[7] as well as developments in super-resolution microscopy.[8]

Lipid membranes are pivotal cellular components, serving roles in intra- and extracellular compartmentalization and as platforms for signal transduction and energy production. Supported lipid membranes, a reconstitution of cellular membranes on a substrate, have been recognized as an effective model for the study of membrane functionalities.[9,10] Surface-sensitive analytical techniques are often used in combination with the supported lipid membranes: fluorescence microscopy is routinely used in laboratories.[11,12] There is a wide choice of fluorescently labelled lipid molecules, as well as fluorescent probes designed to measure membrane properties such as phase[13,14] and viscosity. While these fluorescent probes are useful, there are still concerns about their photostability and possible inhibition of lipid molecule dynamics when incorporated in lipid membranes. In addition, the fact that we need to focus on an extremely thin layer makes the observation of supported lipid membranes particularly difficult, requiring complex equipment such as confocal laser scanning microscopes and total internal reflection fluorescence microscopes. Here, we report the direct imaging of supported lipid membranes on an indium tin oxide (ITO) electrode using ECL of $[Ru(bpy)_3]^{2+}$/tri-*n*-propylamine (TPrA). In principle, ECL can confine the luminescent layer to the vicinity of the supporting electrode, allowing us to observe the surface of lipid membranes with relatively simple equipment – a general microscope and a voltage application device. In fact, electrochemical measurements such as cyclic voltammetry and impedance spectroscopy have been extensively used to characterise supported lipid membranes.[15,16] These techniques can provide electrical properties of membranes, including capacitance, resistance, surface charge, and ion transport, although they lack spatial information. Therefore, the development of ECL imaging on a lipid membrane may also overcome certain limitations of the conventional electrochemical methods. Recently, Trad *et al.*, as well as our group have reported the ECL imaging of antimicrobial peptide (AMP) actions using model lipid membranes.[17,18] AMPs adhere and induce pores on a membrane, changing the ECL emission across the membranes. This suggests that the further investigation of the ECL reactions on lipid membranes could open the way to visualize the molecular characteristics of lipid membranes without the need for labels.

In this study, we prepared several types of lipid membranes: 1,2-dioleoyl-*sn-glycero*-3-phosphocholine (DOPC), and DOPC mixed with either cholesterol, DOTAP (1,2-dioleoyl-3-trimethylammonium-propane), or DOPS (1,2-dioleoyl-*sn-glycero*-3-phospho-L-serine) in a 70 : 30 molar ratio. DOPC is a zwitterionic phospholipid with two unsaturated fatty acid chains, widely used to mimic fluid cell membranes. Cholesterol, an abundant lipid in cell membranes, integrates into the acyl chains of DOPCs, structurally creating a condensed environment within the bilayer.[19,20] DOTAP and DOPS, contrary to the neutral DOPC, possess charged head groups, conferring either a positive or negative charge to the surface of the lipid bilayer. By conducting ECL imaging with

[a] *Frontier Research Institute for Interdisciplinary Sciences, Tohoku University, 980-8578, Aramaki-aza-Aoba, Sendai, Japan. E-mail: kaoru.hiramoto.b4@tohoku.ac.jp*
[b] *Research Institute of Electrical Communications, Tohoku University, Sendai, Japan*
[c] *Advanced Institute for Materials Research, Tohoku University, Sendai, Japan*
[d] *School of Engineering, Tohoku University, Sendai, Japan*

† Electronic supplementary information (ESI) available. See DOI: https://doi.org/10.1039/d4cc06245k

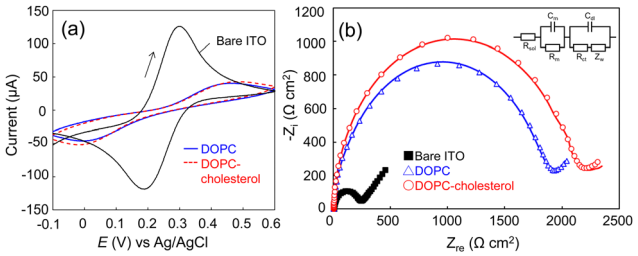

Fig. 1 Electrochemical characterization of the lipid membrane-formed electrodes. (a) CVs of bare ITO, DOPC membrane-formed, and DOPC–cholesterol membrane-formed electrodes (scan rate: 0.1 V s^{-1}). (b) Nyquist plots of the same electrodes in (a). The inset is the equivalent circuit used to fit the experimental data where C_m and R_m are the membrane capacitance and resistance, R_{sol} is the solution resistance, R_{ct} is the charge transfer resistance, Z_w is the Warburg impedance, and C_{dl} refers to the capacitance of the electric double layer.

these mixed lipid compositions, we explored the capability of ECL microscopy to visualize the molecular features of the lipid membranes.

The supported lipid membranes were formed on an ITO electrode *via* a vesicle fusion method (ESI†). Dulbecco's phosphate buffered saline (D-PBS) was used throughout the study as the buffer to support the lipid membranes, except for the formation of the DOPC–DOPS membrane where we added 1 mM Ca^{2+} to the buffer during the vesicle fusion process. The divalent ions were expected to bridge the electrode surface and the negatively charged DOPS head group that could repel each other. The addition of Ca^{2+} ions successfully led to the formation of a DOPC–DOPS bilayer with higher resistance (Fig. S1, ESI†). Firstly, we assessed the quality of the lipid membranes through electrochemical measurements. Fig. 1a and b display the cyclic voltammograms (CV) and spectra of electrochemical impedance spectroscopy (EIS) of the bare ITO, DOPC, and DOPC–cholesterol formed electrodes, respectively. The CV data revealed that the redox peaks of $[Fe(CN)_6]^{3-/4-}$ were shifted and diminished on the lipid membrane-formed electrode, signifying the inhibition of mediator diffusion by the lipid bilayer.[21] This observation is consistent with the enlarged semicircle radius in the Nyquist plot (Fig. 1b), indicating an increase in electrical resistance. The EIS spectra were analysed using Randle's equivalent circuit, as depicted in the inset of Fig. 1b. Based on the EIS data, the membrane resistance for DOPC and DOPC–cholesterol bilayer-formed electrodes were determined to be 1760 ± 64 and 2160 ± 55 Ω cm^2, respectively, indicating the lipid bilayer formation and the packing effect of cholesterol. The membrane capacitance was calculated to be 10.2 ± 0.4 and 9.6 ± 0.2 μF cm^{-2}, respectively. The capacitance exceeded the typical specific capacitance of biological membranes, which is reported to range from 0.8 to 1 μF cm^{-2}. This may be attributed to the defects in the membranes, due to the relatively rough ITO electrode surface.

ECL imaging of the lipid membranes was then performed. The buffer was exchanged to the ECL solution containing 400 μM $[Ru(bpy)_3]^{2+}$ and 25 mM TPrA in D-PBS. The lipid membrane-formed ITO electrode was placed on a microscope stage, with an Ag/AgCl wire and a Pt foil inserted into the drop of ECL solution

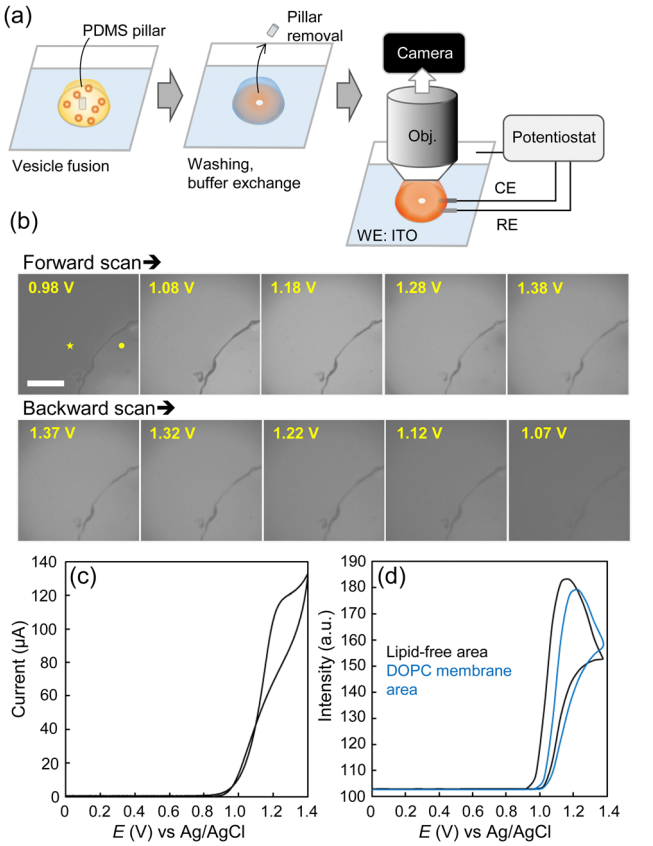

Fig. 2 ECL imaging of the DOPC membrane-formed electrode. (a) Schematic of the ECL imaging. (b) Representative ECL images captured during CV (exposure time: 0.5 s). The interior of the quarter-circle represents the lipid-free area (●) while the exterior is the DOPC membrane-formed area (★). Scale bar: 100 μm. (c) Current and (d) ECL intensity profiles during CV on a DOPC bilayer-coated electrode, at a scan rate of 0.1 V s^{-1}.

for the reference and counter electrodes, respectively. The planar surface of the membrane was observed through the immersion objective and captured with an sCMOS camera while sweeping the voltage from 0 to 1.4 V (Fig. 2a and Fig. S2, ESI†). To differentiate the lipid membrane surface, a lipid-free area (an area devoid of the lipid bilayer) was created by placing a polydimethylsiloxane (PDMS) pillar on the ITO electrode during the vesicle fusion process. The pillar was removed during the observation.

Fig. 2 presents a sequence of ECL images of the DOPC membrane as well as the traces of ECL intensities and current values during CV. Within these images, the interior of the quarter-circle represents the lipid-free area while the exterior is the DOPC membrane formed area. We assume that the dark boundaries may be attributed to the aggregation of lipid molecules. Initially, the lipid-free area exhibited luminescence, followed by the DOPC area. Specifically, in the lipid-free area, the onset of ECL emission was observed at 0.97 V, with the emission peak occurring at 1.17 V. Meanwhile, within the DOPC area, the ECL intensity trace was shifted by approximately 0.05 V, with a 23% reduction in intensity at the peak potential (1.22 V). During reverse scanning, the ECL emission decreased, initially in the DOPC area and subsequently in the

lipid-free area, along with a potential decrease. The ECL images demonstrate the higher resistance of the DOPC area, which inhibited the electrode reactions of $[Ru(bpy)_3]^{2+}$ and TPrA. Nevertheless, the ECL emission was still observed from the membrane owing to the hydrophobic TPrA molecules that can potentially permeate the membrane. In addition, the entire electrode area was not completely covered by the lipid membrane, which could allow $[Ru(bpy)_3]^{2+}$ to diffuse under the lipid membranes to contribute to the ECL reactions. In general, there are three proposed pathways for $[Ru(bpy)_3]^{2+}$/TPrA to undergo ECL emission:[22] the low-oxidation potential route, the oxidative-reduction route, and the catalytic route (Scheme S1, ESI†). Since the concentration of TPrA used here was relatively high compared to that of $[Ru(bpy)_3]^{2+}$, we assume that the first two routes, involving heterogeneous electrode reactions of $[Ru(bpy)_3]^{2+}$ and/or TPrA followed by homogeneous reactions of the TPrA radicals and $[Ru(bpy)_3]^{2+}$ or $[Ru(bpy)_3]^{3+}$ mainly contribute to the emission across the membranes.[23] The previous studies using liposomes showed very little leakage of $[Ru(bpy)_3]^{2+}$ across the lipid bilayer,[7,24] conversely, the lipid membranes in this study were suggested to form loosely organized structures, and thus exhibit inherent ECL emission. Since $[Ru(bpy)_3]^{2+}$ itself exhibits photoluminescence, we examined the appearance of a lipid membrane under a fluorescence microscope (Fig. S3, ESI†). Due to freely diffusing $[Ru(bpy)_3]^{2+}$ ions, fluorescence of the entire solution was observed, but the surface of the lipid membrane could not be distinguished. This demonstrates the advantage of ECL imaging in localizing luminescence close to the electrode surface, allowing thin lipid membranes to be observed without labelling the lipid molecules.

We then conducted ECL imaging on lipid mixtures of DOPC–cholesterol, DOPC–DOTAP, and DOPC–DOPS membranes. Fig. 3 summarizes the ECL behaviours on each membrane. The oxidation currents of $[Ru(bpy)_3]^{2+}$ decreased in the order of DOPC–DOPS, DOPC, DOPC–cholesterol, and DOPC–DOTAP (Fig. S4, ESI†). Specifically, the peak ECL intensity decreased at the DOPC–cholesterol membrane, indicating a higher resistance of this membrane associated with the packing effect of cholesterol (Fig. 3b). On the DOPC–DOTAP membrane, the oxidation of $[Ru(bpy)_3]^{2+}$ was significantly reduced, indicating electrostatic repulsion between the positively charged DOTAP head group and $[Ru(bpy)_3]^{2+}$ ions. This trend was consistent with the ECL images on the membranes, which showed reduced ECL emission at applied potential (Fig. 3c). In addition, the DOPC–DOTAP bilayer was easily detached from the electrode after multiple scans to a positive potential, suggesting that electrostatic repulsion also occurred between the membrane and the electrode surface (Fig. S5, ESI†). On the other hand, DOPC–DOPS showed enhanced ECL emission as well as a shift of the onset potential to negative compared to the DOPC-only membrane (Fig. 3d). CVs of $[Ru(bpy)_3]^{2+}$ and TPrA on the DOPS membrane showed a slight increase in the current at the onset potential range (0.9–1.0 V as magnified in Fig. S4, ESI†) but the increase in ECL intensity in this range was much higher. From this observation, we assume that $[Ru(bpy)_3]^{2+}$ ions and TPrA molecules preferentially coordinate in/on the DOPS membrane so that the homogenous reaction of these molecules was promoted, leading to the enhancement of

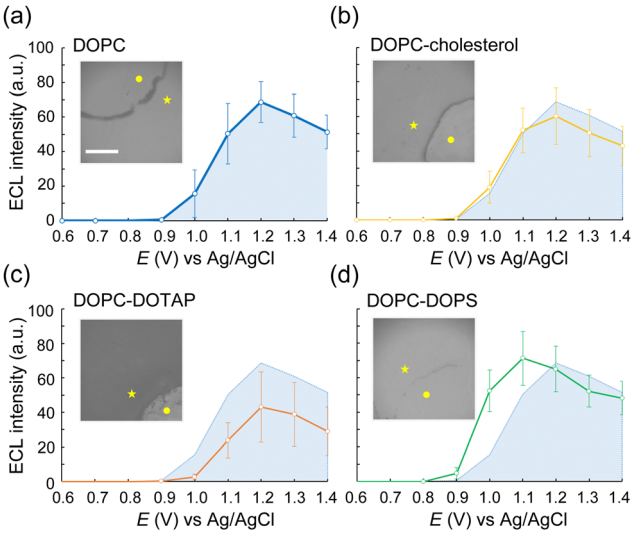

Fig. 3 ECL imaging of electrodes with different types of lipid membranes. (a)–(d) Average ECL intensities on each membrane during a CV scan. DOPC (n = 10), DOPC–cholesterol (n = 9), DOPC–DOTAP (n = 5) and DOPC–DOPS (n = 6). Error bars indicate standard deviation. The light blue shading indicates the average ECL intensity of DOPC. The inset images show the representative ECL images taken at 1.03 V. The interior of the quarter-circle represents the lipid-free area (●), while the exterior is the lipid membrane-formed area (★). Scale bar: 100 μm.

the ECL emission. Consequently, we assume ECL emission through the lipid membranes as shown in Scheme 1: the emission triggered by the direct electrochemical oxidation of TPrA, followed by the homogeneous reactions of TPrA radicals and $[Ru(bpy)_3]^{2+}$ through the membranes. The penetration or the accumulation of $[Ru(bpy)_3]^{2+}$ ions may be modulated by the electrostatic interactions of the lipid head groups or the packing effect, exhibiting inherent ECL emission among the different types of lipid membranes. The remaining technical issue here is that we could not further investigate in which part the ECL molecules coordinate in the lipid membranes. For a thorough investigation, the luminol/H_2O_2 system, which uses neutral and less hydrophobic molecules, can be used to see the effect of electrostatic interactions between the luminophores and lipid molecules. In addition, maintaining the membrane consistency between different types of lipid compositions is important, as the ECL emission through the lipid membranes is largely affected by the defects of the membrane. The quality of the membranes can be improved by using metal substrates – which have relatively low

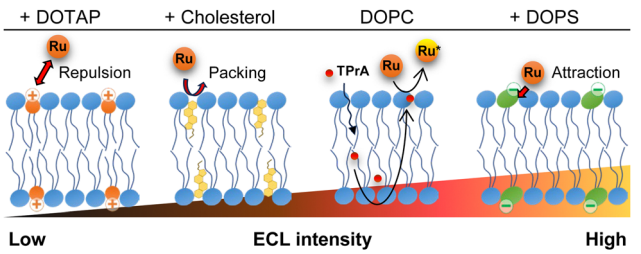

Scheme 1 Possible mechanism of ECL of the $[Ru(bpy)_3]^{2+}$/TPrA system on the lipid membrane-formed electrodes.

roughness compared to ITO electrodes – and tethered lipid membranes[25,26] and/or polymer-supported lipid membranes to achieve higher membrane integrity. The uniqueness of ECL imaging is that differences between lipid membranes are expressed not only by differences in intensity, but also by shifts in the onset potential for luminescence initiation, as shown in Fig. 3. This spectroscopic ECL technique is easily performed by voltage sweep, which we believe can potentially display heterogeneity within lipid membranes such as lipid phase and microdomains.

Finally, we investigated the optimum potential application for the ECL imaging of lipid membranes. Fig. S6 (ESI†) shows the representative ECL images of the DOPC–cholesterol membrane under a constant potential or triangular waves (scan rate: 2 V s^{-1}). Under a constant potential, the boundary between the lipid-free area and the lipid membrane area became blurred when the voltage was above 1.2 V. This may be due to the diffusion of $[Ru(bpy)_3]^{2+/3+}$ ions across the lipid membrane. In the case of 1.1 V, TPrA oxidation was dominant, and due to the short half-life of oxidized TPrA radicals, the emitting layer did not grow. When we applied triangular waves with a relatively high scan rate, it can also reduce the diffusion layer of $[Ru(bpy)_3]^{2+/3+}$ ions, so that the lipid free area and the lipid membrane area could be clearly distinguished even at higher potential.

In summary, we applied ECL of $[Ru(bpy)_3]^{2+}$/TPrA for the direct imaging of lipid membranes with different lipid compositions. The ECL emission across the lipid membrane varied between the charges of the lipid head groups and packing with cholesterol, due to the inherent permeability and reactivity of $[Ru(bpy)_3]^{2+}$ and TPrA. Although the lipid membranes formed in this study require further refinement to represent biological membranes, particularly concerning their integrity, this study provides a straightforward way to image and characterize lipid membranes. In the future, attempts will be made to use ECL imaging of living cells and cellular components to reveal the characteristics of their membranes.

This work was supported by Grant-in-Aid for Scientific Research (No. 23K13770) from the Japan Society for the Promotion of Science (JSPS), the Asahi Glass Foundation, and the Kao Foundation for Arts and Sciences. The authors thank Ms Kazue Arai and Ms Manraibaatar Narantsetseg for the experimental support.

Data availability

The data supporting this article have been included as part of the ESI.†

Conflicts of interest

There are no conflicts to declare.

Notes and references

1 K. Hiramoto, E. Villani, T. Iwama, K. Komatsu, S. Inagi, K. Y. Inoue, Y. Nashimoto, K. Ino and H. Shiku, *Micromachines*, 2020, **11**, 530.
2 Z. Zhang, C. Ma, Q. Xu and J.-J. Zhu, *Analyst*, 2022, **147**, 2884–2894.
3 S. Knezevic, L. Bouffier, B. Liu, D. Jiang and N. Sojic, *Curr. Opin. Electrochem.*, 2022, **35**, 101096.
4 C. Ma, W. Wu, L. Li, S. Wu, J. Zhang, Z. Chen and J.-J. Zhu, *Chem. Sci.*, 2018, **9**, 6167–6175.
5 H. Ding, W. Guo and B. Su, *Angew. Chem., Int. Ed.*, 2020, **59**, 449–456.
6 Y. Ma, C. Colin, J. Descamps, S. Arbault and N. Sojic, *Angew. Chem., Int. Ed.*, 2021, **60**, 18742–18749.
7 F. Ben Trad, V. Wieczny, J. Delacotte, M. Morel, M. Guille-Collignon, S. Arbault, F. Lemaître, N. Sojic, E. Labbé and O. Buriez, *Anal. Chem.*, 2022, **94**, 1686–1696.
8 J. Dong, Y. Lu, Y. Xu, F. Chen, J. Yang, Y. Chen and J. Feng, *Nature*, 2021, **596**, 244–249.
9 E. T. Castellana and P. S. Cremer, *Surf. Sci. Rep.*, 2006, **61**, 429–444.
10 M. Komiya, M. Kato, D. Tadaki, T. Ma, H. Yamamoto, R. Tero, Y. Tozawa, M. Niwano and A. Hirano-Iwata, *Chem. Rec.*, 2020, **20**, 730–742.
11 F. Pincet, V. Adrien, R. Yang, J. Delacotte, J. E. Rothman, W. Urbach and D. Tareste, *PLoS One*, 2016, **11**, e0158457.
12 T. Baumgart, G. Hunt, E. R. Farkas, W. W. Webb and G. W. Feigenson, *Biochim. Biophys. Acta*, 2007, **1768**, 2182–2194.
13 H.-J. Kaiser, D. Lingwood, I. Levental, J. L. Sampaio, L. Kalvodova, L. Rajendran and K. Simons, *Proc. Natl. Acad. Sci. U. S. A.*, 2009, **106**, 16645–16650.
14 Y. Okamoto, K. Hamaguchi, M. Watanabe, N. Watanabe and H. Umakoshi, *Membranes*, 2022, **12**, 770.
15 G. Valincius, T. Meškauskas and F. Ivanauskas, *Langmuir*, 2012, **28**, 977–990.
16 Z. Su, J. J. Leitch and J. Lipkowski, *Curr. Opin. Electrochem.*, 2018, **12**, 60–72.
17 F. Ben Trad, J. Delacotte, M. Guille-Collignon, F. Lemaître, S. Arbault, N. Sojic, F. Burlina, E. Labbé and O. Buriez, *Chem. Biomed. Imaging*, 2023, **1**, 58–65.
18 K. Hiramoto, K. Ino, I. Takahashi, A. Hirano-Iwata and H. Shiku, *Faraday Discuss.*, 2024, DOI: **10.1039/D4FD00137K**.
19 S. L. Veatch and S. L. Keller, *Biophys. J.*, 2003, **85**, 3074–3083.
20 Y. Zhang, Q. Li, M. Dong and X. Han, *Colloids Surf., B*, 2020, **196**, 111353.
21 E. Labbé and O. Buriez, *Electrochem. Sci. Adv.*, 2022, **2**, e2100170.
22 W. Miao, J.-P. Choi and A. J. Bard, *J. Am. Chem. Soc.*, 2002, **124**, 14478–14485.
23 W.-X. Fu, P. Zhou, W.-L. Guo and B. Su, *Adv. Sens. Energy Mater.*, 2022, **1**, 100028.
24 W. Zhan and A. J. Bard, *Anal. Chem.*, 2006, **78**, 726–733.
25 D. J. McGillivray, G. Valincius, D. J. Vanderah, W. Febo-Ayala, J. T. Woodward, F. Heinrich, J. J. Kasianowicz and M. Lösche, *Biointerphases*, 2007, **2**, 21–33.
26 I. Gabriunaite, G. Valincius, A. Žilinskas and A. Valiūnienė, *J. Electrochem. Soc.*, 2022, **169**, 037515.

